Magnetic field free circularly polarized thermal emission from a chiral metasurface

S. A. Dyakov,[1,*] V. A. Semenenko,[1] N. A. Gippius,[1] and S. G. Tikhodeev[2,3]

[1]*Skolkovo Institute of Science and Technology, 143025 Moscow Region, Russia*
[2]*A. M. Prokhorov General Physics Institute, RAS, Vavilova 38, 119991 Moscow, Russia*
[3]*Faculty of Physics, Lomonosov Moscow State University, 119991 Moscow, Russia*

Thermal radiation from bulk disorderly placed nonresonant emitters is incoherent broadband and isotropic. In an external magnetic field the thermal radiation from any source is circularly polarized. Here we propose a thermal radiation source which emits circularly polarized radiation and which is not placed in a magnetic field. The thermal source consists of a slab waveguide with etched chiral metasurface of fourfold rotational symmetry. Using the Fourier modal method we analyze the eigenmodes of the structure and the emissivity spectra. We demonstrate that due to the absence of a mirror symmetry of the metasurface its eigenmodes as well as the thermally generated electromagnetic waves become circularly polarized. In this paper we discuss the origin of this phenomenon in detail. We demonstrate that the degree of circular polarization in an optimized structure can be as high as 0.87.

I. INTRODUCTION

In the last years, the study of far-field and near-field thermal emission of artificial materials attracted a great deal of attention from researchers due to its high potential for important applications in near-field thermal management [1–20], energy harvesting [21–24], and coherent thermal sources [25–38]. In Ref. [25] it was demonstrated that a periodically microstructured surface can emit coherent and linearly polarized thermal emission, that opened the perspective for control of the spectral [31,37,39–42], angular [43,44], coherence [25,45], and polarization characteristics [46–52] of thermal radiation. The angular emission diagram and the polarization of thermal radiation are dictated by the emitter symmetry. In particular, a structure which lacks a mirror symmetry can generate circularly polarized thermal radiation. The mirror symmetry can be broken down by applying an external magnetic field due to spin-orbit interaction of electrons [53,54]. This phenomenon is known as magneto-optic Kerr effect and explains, for instance, the strong circular polarization of white dwarf emission [55]. The circularly polarized thermal radiation in a magnetic field has been observed in a laboratory too (see for example Refs. [56,57]). Another way to break down the mirror symmetry is to create a structure with a chiral morphology.

The possibility of chiral structures for circular polarization filtering was widely studied in the literature [58–68]. In Refs. [64–66] it was shown that the three-dimensional chiral photonic crystal structures show giant circular dichroism at telecommunication wavelengths due to their polarization dependent photonic stop bands and can be used as filters for circular polarization. Such structures can have wide operation range but demand a complex fabrication technique. To overcome this problem, one can use a chiral metasurface which requires only a single layer of lithography.

The transmission characteristics of a metasurface are evoked by the type of its chiral morphology [53]. Structures with twofold rotational symmetry (C_2) demonstrate strong circular dichroism in transmission [69]. This phenomenon can be used for design of circular polarization filters for thermal radiation from heated objects. For instance, in Ref. [47] it was demonstrated that the chiral silicon metasurfaces based on infrared Fano resonances can transmit only one of the two circular polarizations in the wavelength range 4–5 μm. One can also use an array of silver zigzag stripes [50] or more complex C_2 symmetrical structures such as a gold pixelized metasurface [70] for obtaining the arbitrary polarized light in the near infrared.

In contrast to C_2 symmetrical structures, metasurfaces with fourfold rotational symmetry can have circular dichroism in transmission along the normal direction due to the lack of an additional mirror symmetry with respect to a plane parallel or perpendicular to the z axis [69]. C_4 symmetrical metasurfaces have been utilized in Refs. [58–62], for obtaining the circularly polarized visible and near infrared photoluminescence of semiconductor quantum dots. The degree of circular polarization (DCP) depends on the surface geometrical parameters and is a matter of theoretical optimization. The highest obtained degree of circular polarization was close to 100% in the optimized structures.

Due to the scalability of optical resonances, the operation range of C_4 symmetrical structures can be shifted up to the middle infrared by increasing their spatial period. In most of the publications, the C_2 symmetrical metasurfaces are considered as infrared filters and, hence, for obtaining the circularly polarized thermal radiation they require a separate thermal source. Moreover, thermal emission passed through the C_2 symmetrical structure also has a linearly polarized fraction [47].

_____
*s.dyakov@skoltech.ru
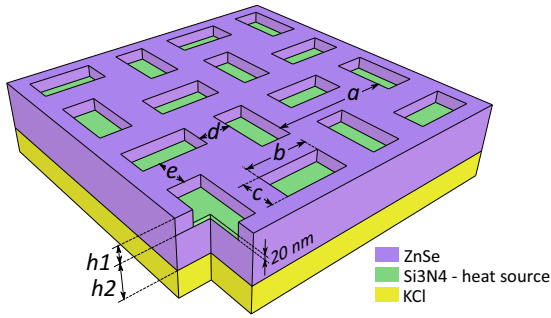
FIG. 1. Schematic of chiral metasurface. The period of the photonic crystal structures is $a = 10\ \mu$m, $b = 2a/5$, $c = a/5$.

In this paper we propose a design of a C_4 symmetrical chiral metasurface which generates circularly polarized thermal radiation itself due to the presence of a specially selected absorbing material and of a high refractive index semiconducting layer with optimized chiral spatial modulation in it. Unlike most of previous papers, we are focused on wavelengths which are close to the maximum of Planck's spectrum at a temperature of 300 K.

II. MODEL STRUCTURE AND THEORY

We propose a thermal emitter consisting of a KCl substrate capped by a ZnSe waveguide with a two-dimensional array of etched rectangles (Fig. 1). The etched pattern has chiral morphology with C_4 rotational symmetry. The bottom surface of rectangles is covered by 20-nm-thick layer of Si_3N_4. In this work we assume that the temperature of the thermal emitter is close to 300 K and hence we are focused on the 7–15-μm wavelength range. The choice of materials ZnSe and KCl is attributed to the fact that they are transparent in the middle infrared and hence do not contribute to the thermal emission in this spectral range. In contrast, Si_3N_4 has a wide absorption band and, therefore, is the only source of thermal radiation in the structure. Dielectric permittivities of all of the above materials have weak dispersion and therefore in calculation we consider them dispersionless in the wavelength range of interest: $\varepsilon(ZnSe) = 5.67$, $\varepsilon(KCl) = 2.08$, and $\varepsilon(Si_3N_4) = 10.5 + 9.2i$.

In this paper, the emissivity is calculated by Kirhoff's law which states that the absorptivity and emissivity are equal. This has been numerically verified for uniform and photonic crystal slabs [71]. In turn, the absorptivity is calculated using the Fourier modal method in the scattering matrix form also known as rigorous coupled wave analysis (RCWA) [72–75]. The decompositions of electric and magnetic fields into Fourier series were done using Li's factorization rules [76] with $13 \times 13 = 169$ spatial harmonics. We checked the accuracy of the method with up to $31 \times 31 = 961$ spatial harmonics for the most important results.

Our choice of RCWA is due to the following facts. First of all, the structure in study is two-dimensionally periodic and hence it is physically justified to expand the electromagnetic field into spatial Fourier harmonics. Second, we calculate the optical properties of an open system which can be problematic for methods such as finite difference time domain (FDTD)

where absorbing boundary conditions or perfectly matched layers are used to limit the computational domain. Third, in our structure, the thickness of the absorbing layer is 30 nm while all other dimensions are of the order of 1 μm; the fine gridding of such a multiscale geometry in differential methods such as FDTD or the finite element method (FEM) can result in extremely long computational times. The comparison of RCWA with other methods [77,78] demonstrates the effectiveness of RCWA in calculating grating structures. Finally, as is shown in Ref. [79] by Li, the RCWA proved itself to be quite efficient for vertically invariant periodic structures (e.g., lamellar gratings) such as our structure. Li's contributions to the method have also given the possibility to improve the differential method applied to an arbitrarily shaped profile, and we employ them in our approach.

III. RESULTS

To estimate the expected circular polarization of thermal emission, we calculate the emissivity spectra of chiral metasurface in left circular polarization (LCP) I_{LCP} and right circular polarization (RCP) I_{RCP} as well as the degree of circular polarization. We estimate the DCP as

$$\rho_c = \frac{I_{RCP} - I_{LCP}}{I_{RCP} + I_{LCP}}. \tag{1}$$

As shown in Fig. 2(a), in the displayed spectral range, the emissivity is characterized by the two peaks both having different amplitudes in LCP and RCP. As a result, the DCP is nonzero and reaches the values of -0.73 and 0.87 at $\lambda = 12.65$ and $13\ \mu$m correspondingly.

To understand the physical origin of the emissivity peaks, we analyze the structure eigenmodes. At first, we use the simplest approach for this, namely, an empty lattice approximation. In this approximation we replace the photonic crystal layer by a uniaxial homogeneous medium (UHM) with diagonal dielectric permittivity tensor. For the sake of simplicity we omit the thin Si_3N_4 layer and replace the rectangular holes in the ZnSe layer by the cylindric ones. In this simplified approximation we lose the chirality of the structure [the symmetry becomes SO(2) instead of C_4] and thus cannot estimate the DCP. But it allows us at least to approximate the energy dispersion of the TE and TM waveguide modes in the structure. For this purpose we roughly estimate the effective ordinary and extraordinary dielectric permittivities of UHM from the generalized Bruggeman formula:

$$\sum_{j=1}^{2} f_j \frac{\varepsilon_{eff} - \varepsilon_j}{\varepsilon_{eff} + L(\varepsilon_j - \varepsilon_{eff})} = 0, \tag{2}$$

where the index $j = 1, 2$ denotes air or ZnSe, ε_j is the dielectric permittivity, f_j is the filling factor, and L is the depolarization factor. We consider the entire effective structure as a dielectric double slab waveguide and find its guided modes. At $k_z = 0$ in the TE polarized guided modes, the electric field is perpendicular to the z axis, while in TM polarization the electric field is approximately parallel to the z axis. Thus, in Eq. (2) we use the depolarization factors typical for the cylindrical inclusions with the cylinder axis oriented along the z axis: $L_{TE} = 1/2$ and $L_{TM} = 0$. The effective dielectric
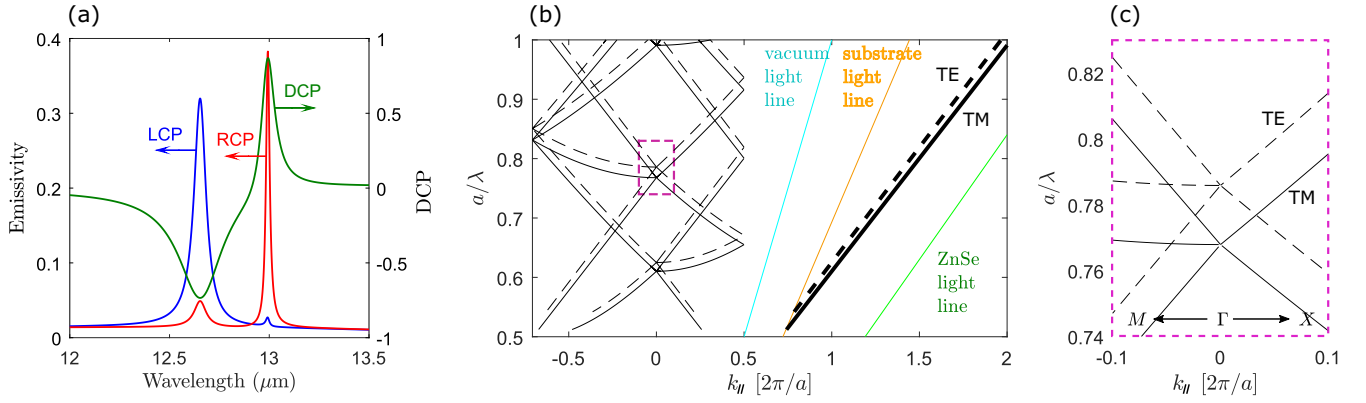
FIG. 2. (a) LCP (blue) and RCP (red) emissivity spectra of the chiral metasurface with $h_1 = 4$ μm and $h_2 = 5$ μm. Degree of circular polarization is shown by green. (b) The lowest TE and TM waveguided modes in an effective homogeneous uniaxial double slab waveguide and the same modes folded into the first Brillouin zone. The dispersion of folded modes is shown along Γ-X and Γ-M directions. $h_1 = 4$ μm, $h_2 = 5$ μm. The modes bounded by the magenta dashed rectangle are shown in panel (c). Arrows show the corresponding photonic crystal directions.

permittivities, obtained from Eq. (2), are [80] $\varepsilon_{\mathrm{eff,TE}} \approx 3.4$ and $\varepsilon_{\mathrm{eff,TM}} \approx 4.2$.

To calculate the eigenmodes of the double slab waveguide we use the equation

$$\left(\frac{\xi_2}{\xi_1 \xi_t} + \frac{\xi_1}{\xi_2 \xi_i}\right) t_1 t_2 + q_1 t_1 + q_2 t_2 = \frac{1}{\xi_i} + \frac{1}{\xi_t}, \qquad (3)$$

where

$$q_\alpha = \frac{1}{\xi_\alpha} - \frac{\xi_\alpha}{\xi_i \xi_t}, \qquad (4)$$

$t_\alpha = \tan k_{z\alpha} h_\alpha$ $(\alpha = 1, 2)$, $\xi_n = k_{zn}/\varepsilon_n$ for TM polarization and $\xi_n = 1/k_{zn}$ for TE polarization; k_{zn} stands for the z component of the wave vector in nth medium, the symbol n denotes i, 1, 2, or t which mean incoming medium, photonic crystal layer, nonmodulated layer, and outgoing medium correspondingly. The z component of the wave vector k_{zn} can be found from the equation $k_x^2 + k_y^2 + k_{zn}^2 = \varepsilon_n k_0^2$, where k_0 is the absolute value of the photon wave vector in vacuum.

The dispersion of eigenmodes of the effective double slab waveguide [shown in Fig. 2(b) by black thick lines] are below the vacuum and substrate light cones and therefore are not visible from the far field. It is noteworthy that due to the different effective dielectric permittivities of UHM in TM and TE polarizations, $\varepsilon_{\mathrm{eff,TM}}$ and $\varepsilon_{\mathrm{eff,TE}}$, the TM guided mode appears to be below the TE guided mode, contrary to the case of isotropic waveguide. The introduction of periodicity folds the dispersion curves into the first Brillouin zone and couples the guided modes with photon continua in vacuum and substrate. In the result, so-called quasiguided modes (often called guided resonance modes) appear [72]. It can be seen from Fig. 2(b) that several families of quasiguided modes are formed in the Γ point. One of these families is shown in Fig. 2(c) on a larger scale near $a/\lambda = 0.78$.

Let us return to the initial periodic structure and demonstrate its eigenmodes and field distributions in them. To do this, we calculate the scattering matrix of the periodic structure, $\mathbb{S}$, which couples the incoming and outgoing amplitude

vectors, $|\mathbf{I}\rangle$ and $|\mathbf{O}\rangle$, as defined in Ref. [72]:

$$|\mathbf{O}\rangle = \mathbb{S}(\lambda, k_x, k_y) |\mathbf{I}\rangle . \qquad (5)$$

By setting the incoming amplitudes as zero, we obtain the following eigenvalue problem [81]:

$$\mathbb{S}^{-1}(\lambda, k_x, k_y) |\mathbf{O}\rangle_{\mathrm{res}} = |0\rangle , \qquad (6)$$
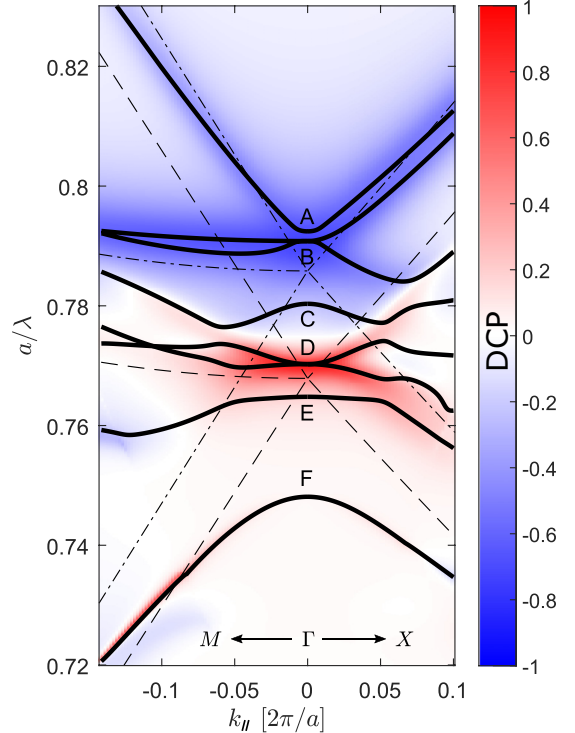
FIG. 3. The calculated dispersion of quasiguided modes octet along Γ-M and Γ-X directions near Γ point (solid lines) against the background of the energy and k_x dependence of the DCP. Color scale is explained on the right. Dashed and dash-dotted lines represent the structure TM and TE eigenmodes in empty lattice approximation. Arrows show the corresponding photonic crystal directions.
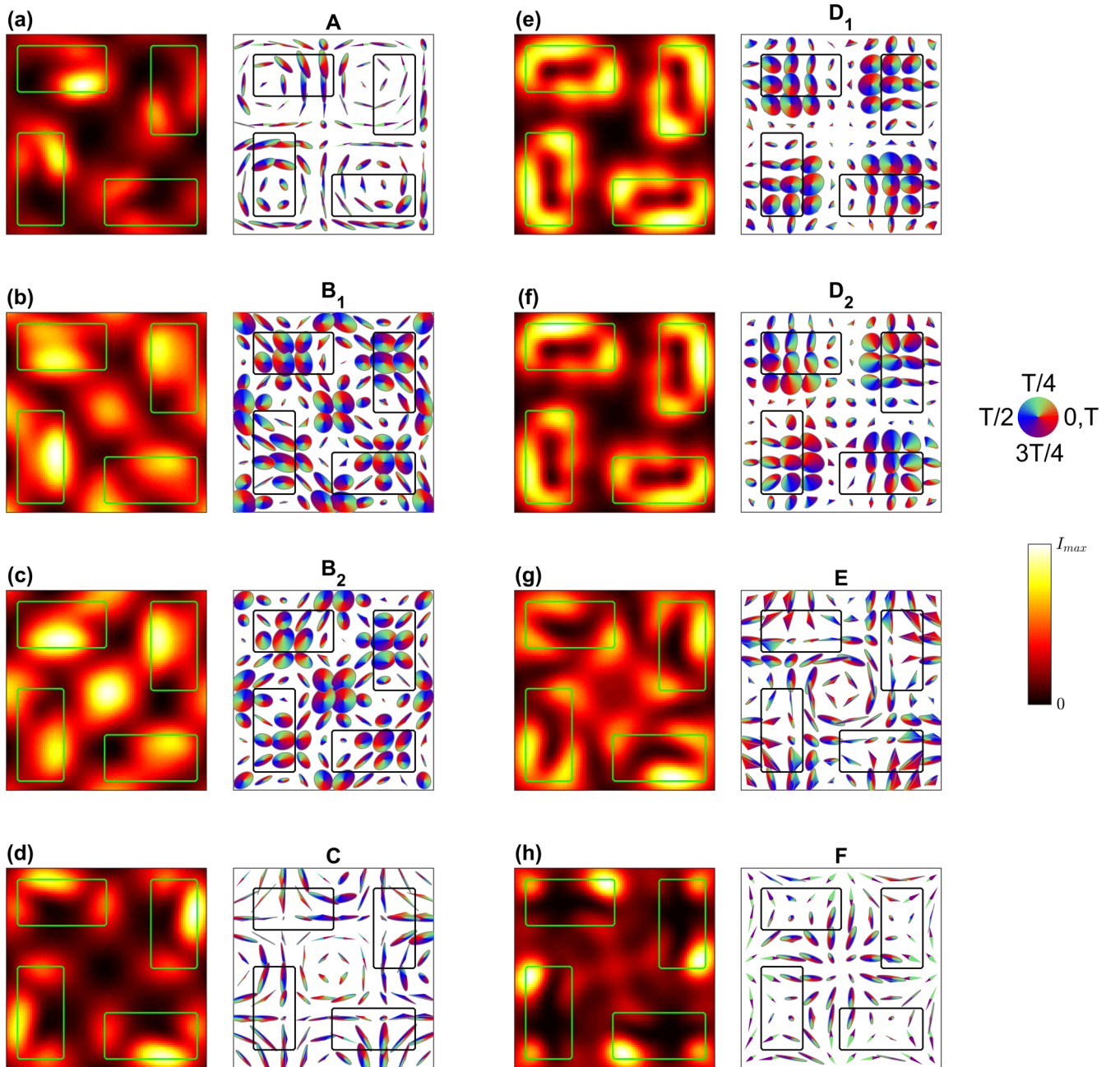
FIG. 4. Left panels: Electric-field intensities of the quasiguided modes A–F in Γ point. The maximal field intensities over the displayed cross sections normalized to those in free space are shown in titles. Right panels: Phase representation of the fields showing their polarization characteristics. Fields are calculated in the middle of the absorbing layer. Green and black lines are material boundaries.

where $|\mathbf{O}\rangle_{\mathrm{res}}$ is the resonant output eigenvector. The eigenmodes of the chiral metasurface are shown in Fig. 3 against the background of the DCP as a function of k_x and a/λ. In comparison to the modes obtained in empty lattice approximation, the degeneracy of the modes in the Γ point is lifted except for two doublets B and D. The picture of such modes is dictated by the structure symmetry C_4 [72]. The highest DCP is reached near doublets B and D. The electric-field distributions in modes A–F are shown in Fig. 4. The left panels in Fig. 4 demonstrate the field intensities. In the right panels the electric-field vectors are shown by the color cones featuring the field polarization

characteristics. In such representation, the cone base denotes the polarization plane, while the cone height is proportional to the product of the electric-field amplitude and the DCP. The color scale represents the phase of electromagnetic oscillations as explained in Fig. 4 See Supplemental Material at [82] for details on the cone representation of electromagnetic field. It is remarkable that in B and D doublets, where the structure emissivity is highly circularly polarized, the eigenfields are also circularly polarized.

The described quasiguided modes of our photonic crystal slab are the Fano type [83,84] resonances as they appear due to
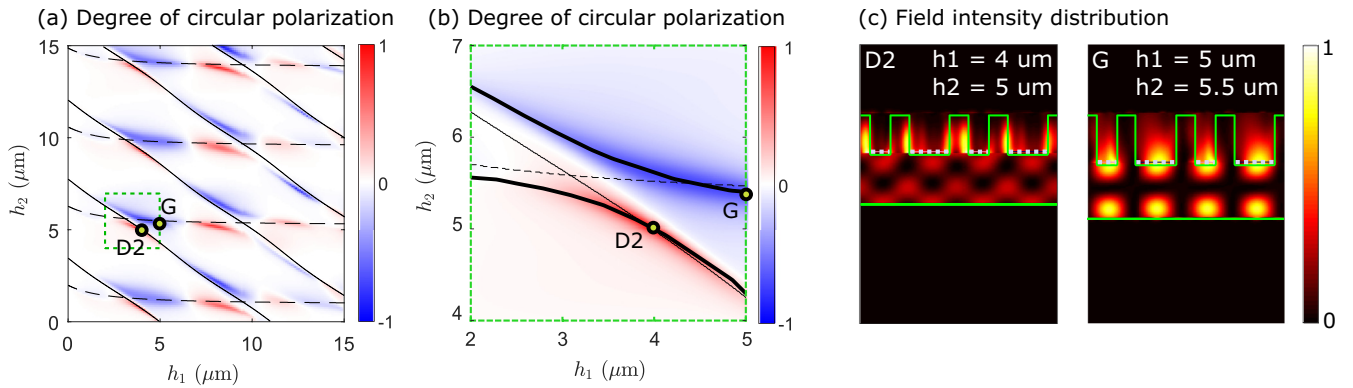
FIG. 5. (a) Degree of circular polarization as a function of thicknesses h_1 and h_2 at $\lambda = 13$ μm. Resonances in empty lattice approximations are shown by dashed lines for TE polariztion and thin solid lines for TM polarization. The modes bounded by the green dashed rectangle are shown in (b). Black thick lines in (b) denote resonances calculated for the initial chiral metasurface. (c) Electric-field intensity of the chiral emitter eigenmodes calculated in the resonances D_2 and G specified in the panel (a). Thermal emitter is shown by dotted lines.

the interaction of the discrete guided modes of the waveguide with the photon continuum in air (see, e.g., in Refs. [72,81]).

As the next step, we calculate the DCP of thermal emission at $\lambda = 13$ μm as a function of the thicknesses of modulated and nonmodulated parts of the structure, h_1 and h_2 [see Fig. 5(a), red-blue image graph and the color map on the right]. It can be seen that the emissivity resonantly depends on the parameters h_1 and h_2. These resonances are attributed to the excitation of lossy quasiguided modes in the periodical ZnSe waveguide [59,72]. They can be approximately described in empty lattice approximation by taking the x and y components of the wave vector in Eq. (3) as $k_x = k_y = 2\pi/a$ which corresponds to the Γ point in the higher-order Brillouin zone of the reciprocal photonic crystal lattice. The solutions of transcendental Eq. (3) are shown in Fig. 5(a) for TE polarization by dashed lines and for TM polarization by solid lines.

From Fig. 5(a) one can see that the resonances in TE and TM polarization have different behavior with change of h_1 and h_2. Indeed, the TE quasiguided modes are practically not affected by the thickness of the photonic crystal slab h_1 while the TM modes depend both on h_1 and h_2. In terms of the empty lattice approximation, such distinction between the modes behavior is originated from the UHM anisotropy. To explain this in more detail, we calculate the photon energies at $k_x = k_y = 2\pi/a$ for the materials of effective double slab waveguide and compare these photon energies with a/λ_0 where $\lambda_0 = 13$ μm (see Table I). By doing so, we fix the energy of guided modes at the value of a/λ_0 like in Fig. 5(a). Inspection of Table I reveals that due to the different $\varepsilon_{\mathrm{eff,TM}}$ and $\varepsilon_{\mathrm{eff,TE}}$, the guided mode of the effective double slab waveguide appears to be above the UHM light cone in TM polarization and below the UHM light cone in TE polarization. This means that in the effective double slab waveguide, the TE guided modes are confined in the homogeneous part of the structure and hence depend only on thickness h_1. In contrast, the TM guided modes are confined both in the photonic crystal and homogeneous parts of the waveguide and depends on h_1 and h_2. Figure 5(c) shows the electric-field intensity distributions in the eigenmodes of the chiral metasurface with h_1 and h_2 which are

close TE and TM resonances calculated in the empty lattice approximation [D_2 and G points in Fig. 5(a)]. It can be seen that, indeed, the electric field is localized in the entire waveguide for the point D_2 and in the modulated part of the waveguide for the point G. Figure 5(b) shows the eigenmodes of initial periodic structure on the $h_1 - h_2$ diagram for $k_x = k_y = 0$ and $\lambda = 13$ μm. It can be seen from Fig. 5(b) that the eigenmodes of the periodic structure are close to the DCP maxima and are split near the intersection between TE and TM eigenmodes of the effective homogeneous double slab waveguide.

IV. DISCUSSIONS

Since the thermal emissivity and absorptivity are equal by Kirchoff's law and the absorptivity is connected with transmission, reflection, and diffraction by the energy conservation law $R + T + A = 1$, the phenomenon of circular polarization of thermal emission from chiral metasurface can be understood in terms of the reflection and transmission coefficients. Please note that in the above formula the reflection and transmission are taken as a sum over all diffraction channels.

At normal incident angle and at wavelength in the range of interest (12–13.5 μm) our structure has open diffraction channels to the KCl substrate and has no diffraction channels to the air [see Fig. 6(a)]. Due to the electrodynamical reciprocity (see, e.g., the discussion in Ref. [60]) its reflection spectra in RCP and LCP are identical [Fig. 6(b)]. In contrast, the

TABLE I. Effective dielectric permittivity of UHM and characteristic energies a/λ of the effective double slide waveguide at $k_x = k_y = 2\pi/a$ compared to a/λ_0.

	TE	TM
Effective epsilon of UHM	3.4	4.5
Light line in vacuum	1.414	
Light line in substrate	0.980	
a/λ_0	0.770	
Light line in UHM	0.771	0.665
Light line in ZnSe	0.594	
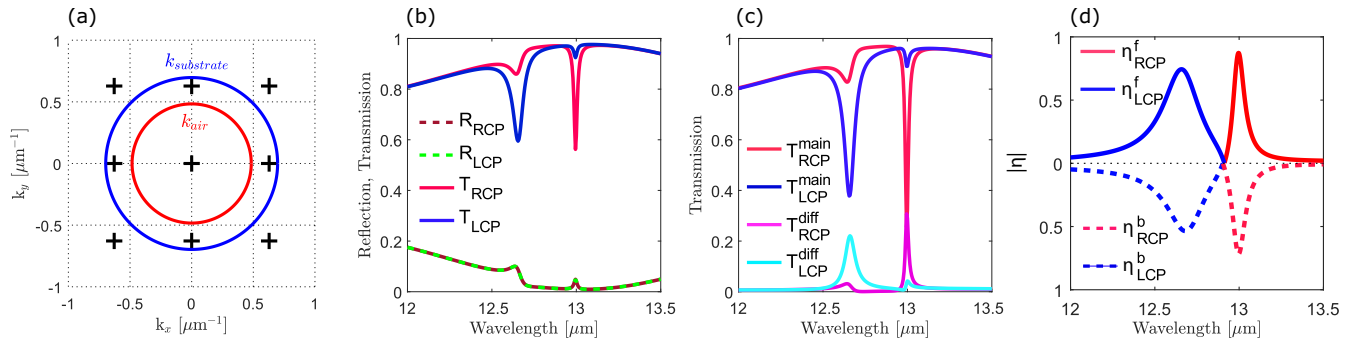
FIG. 6. (a) The map of Bragg harmonics of the $k_x = k_y = 0$ incoming light. Red and blue lines show the air and substrate line cone cross sections for $\lambda = 13~\mu$m. (b) Reflection and transmission spectra in RCP and LCP summed over all transmission channels of the $k_x = k_y = 0$ incoming light. (c) Transmission spectra in RCP and LCP in main diffraction channel (red and blue lines) and in high-order diffraction channels (magenta and cyan lines). (d) Degree of circular polarization of thermal emission from chiral metasurface calculated towards air half space (solid lines) and substrate half space (dashed lines). Blue and red colors represent RCP and LCP parts of thermal emission respectively. For the substrate half space, the curves are flipped with respect to horizontal line $\rho_c = 0$.

transmission spectra along the normal direction are different in RCP and LCP, which for our C_4 symmetrical structure is explained by the absorption losses in the emitting layer with Si_3N_4 and by the diffraction into the substrate. The intensities of light transmitted through the chiral metasurface to the substrate main channel and to all open diffraction channels are shown in Fig. 6(c). It can be seen that both types of transmission are characterized by the strong circular dichroism. The resulted degree of circular polarization is shown in Fig. 6(d) by solid lines.

So far, we have studied the thermal emission towards the upper air half space which terminates the chiral metasurface on its periodic side. In this regard, it is interesting to see the polarization state of thermal emission towards the substrate. For this, we calculated the LCP and RCP absorptivity (i.e.,

emissivity) spectra for the light which is coming in to the structure from the substrate side. The corresponding degree of circular polarization of thermal emission is shown in Fig. 6(d) by dashed lines. It can be seen in Fig. 6(d), that, in spite of the fact that the chiral twist (right or left) of the metasurface geometry is not invariant of the light propagation direction, the degrees of circular polarization of thermal emission to upper and lower half spaces are almost the same.

In terms of the Stokes polarization vector (S_0, S_1, S_2, S_3), the degree of circular polarization calculated by formula (1) and shown in Fig. 6(d) is equal to the ratio of S_3/S_0. Due to the fact that our C_4 symmetrical metasurface has identical reflection and transmission spectra in both linear polarizations, the components of Stokes vector S_1 and S_2 are equal to zero. It means that the polarized fraction of thermal emission from our structure is represented solely by circularly polarized waves. This is a common property of all C_4 symmetrical structures which lack an additional mirror symmetry.

Finally, the angular emission diagram of thermal radiation is shown in Fig. 7 for $\lambda = 13~\mu$m in two circular polarizations. The bright spot and the lines in Fig. 7 correspond to the quasiguided modes D. We notice that in accordance with the dispersions of quasiguided modes shown in Fig. 3, the directionality of right circularly polarized thermal emission is highly pronounced.

V. CONCLUSION

In conclusion, we have demonstrated the chiral metasurface that can emit the circularly polarized thermal radiation to the air half space and to the substrate half space. Both parts of thermal emission are strongly circularly polarized with the degree of circular polarization up to 87%. We attribute this effect to the C_4 symmetry of the photonic crystal part of the structure. Due to the lack of mirror symmetry, the eigenmodes of this metasurface are circularly polarized. The circularly polarized thermal emission is highly directional.

Directionality of thermal emission
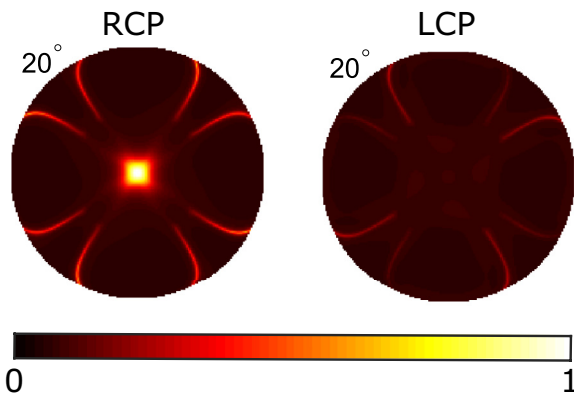
FIG. 7. Polar plots of the angular dependencies of thermal emission intensity in RCP (left panel) and LCP (right panel) calculated for $h_1 = 4~\mu$m, $h_2 = 5~\mu$m. In the displayed polar plots, the polar angle of thermal emission direction (i.e., the angle between the wave vector and z axis) is represented by the distance from the pole ρ, while the azimuthal angle (i.e., the angle between the xy projection of the wave vector and the x axis) is represented by angular coordinate φ. The thermal emission intensity is calculated for polar angles between 0° and 20°.

[1] P. Ben-Abdallah, AIP Adv. **7**, 065002 (2017).

[2] K. Kim, B. Song, V. Fernández-Hurtado, W. Lee, W. Jeong, L. Cui, D. Thompson, J. Feist, M. H. Reid, F. J. García-Vidal *et al.*, Nature (London) **528**, 387 (2015).

[3] A. Ghanekar, Y. Tian, M. Ricci, S. Zhang, O. Gregory, and Y. Zheng, Opt. Express **26**, A209 (2018).

[4] P. Ben-Abdallah and S.-A. Biehs, Phys. Rev. B **94**, 241401 (2016).

[5] P. Ben-Abdallah, Phys. Rev. Lett. **116**, 084301 (2016).

[6] S. A. Dyakov, J. Dai, M. Yan, and M. Qiu, J. Phys. D **48**, 305104 (2015).

[7] B. Song, D. Thompson, A. Fiorino, Y. Ganjeh, P. Reddy, and E. Meyhofer, Nat. Nanotechnol. **11**, 509 (2016).

[8] S. A. Dyakov, J. Dai, M. Yan, and M. Qiu, Appl. Phys. Lett. **106**, 064103 (2015).

[9] P. Ben-Abdallah, A. Belarouci, L. Frechette, and S.-A. Biehs, Appl. Phys. Lett. **107**, 053109 (2015).

[10] S. A. Dyakov, J. Dai, M. Yan, and M. Qiu, Phys. Rev. B **90**, 045414 (2014).

[11] F. Singer, Y. Ezzahri, and K. Joulain, J. Quant. Spectrosc. Radiat. Transfer **154**, 55 (2015).

[12] J. Dai, S. A. Dyakov, and M. Yan, Phys. Rev. B **92**, 035419 (2015).

[13] C. Lin, B. Wang, K. H. Teo, and Z. Zhang, J. Appl. Phys. **122**, 143102 (2017).

[14] M. Mirmoosa, M. Omelyanovich, and C. Simovski, J. Opt. **18**, 115104 (2016).

[15] M. Lim, J. Song, J. Kim, S. S. Lee, I. Lee, and B. J. Lee, J. Quant. Spectrosc. Radiat. Transfer **210**, 35 (2018).

[16] Y. Yang and L. Wang, J. Quant. Spectrosc. Radiat. Transfer **197**, 68 (2017).

[17] S. Basu, Y. Yang, and L. Wang, Appl. Phys. Lett. **106**, 033106 (2015).

[18] J. Dai, S. A. Dyakov, S. I. Bozhevolnyi, and M. Yan, Phys. Rev. B **94**, 125431 (2016).

[19] Y. Guo and Z. Jacob, Opt. Express **21**, 15014 (2013).

[20] J. Dai, S. A. Dyakov, and M. Yan, Phys. Rev. B **93**, 155403 (2016).

[21] E. Rephaeli and S. Fan, Opt. Express **17**, 15145 (2009).

[22] S. Fan, Nat. Nanotechnol. **9**, 92 (2014).

[23] A. Lenert, D. M. Bierman, Y. Nam, W. R. Chan, I. Celanović, M. Soljačić, and E. N. Wang, Nat. Nanotechnol. **9**, 126 (2014).

[24] D. M. Bierman, A. Lenert, W. R. Chan, B. Bhatia, I. Celanović, M. Soljačić, and E. N. Wang, Nat. Energy **1**, 16068 (2016).

[25] J.-J. Greffet, R. Carminati, K. Joulain, J.-P. Mulet, S. Mainguy, and Y. Chen, Nature (London) **416**, 61 (2002).

[26] Y. Guo, C. L. Cortes, S. Molesky, and Z. Jacob, Appl. Phys. Lett. **101**, 131106 (2012).

[27] L. Wang and Z. Zhang, J. Heat Transfer **135**, 091505 (2013).

[28] V. Pipa, A. Liptuga, and V. Morozhenko, J. Opt. **15**, 075104 (2013).

[29] S. Maruyama, T. Kashiwa, H. Yugami, and M. Esashi, Appl. Phys. Lett. **79**, 1393 (2001).

[30] F. Marquier, K. Joulain, J.-P. Mulet, R. Carminati, J.-J. Greffet, and Y. Chen, Phys. Rev. B **69**, 155412 (2004).

[31] H. Sai, Y. Kanamori, and H. Yugami, Appl. Phys. Lett. **82**, 1685 (2003).

[32] S. S. Kruk, Z. J. Wong, E. Pshenay-Severin, K. O'brien, D. N. Neshev, Y. S. Kivshar, and X. Zhang, Nat. Commun. **7**, 11329 (2016).

[33] A. Narayanaswamy and G. Chen, Phys. Rev. B **70**, 125101 (2004).

[34] R. Biswas, C. G. Ding, I. Puscasu, M. Pralle, M. McNeal, J. Daly, A. Greenwald, and E. Johnson, Phys. Rev. B **74**, 045107 (2006).

[35] M. A. Kats, R. Blanchard, S. Zhang, P. Genevet, C. Ko, S. Ramanathan, and F. Capasso, Phys. Rev. X **3**, 041004 (2013).

[36] H. Sai, Y. Kanamori, and H. Yugami, J. Micromech. Microeng. **15**, S243 (2005).

[37] H. Sai, H. Yugami, Y. Akiyama, Y. Kanamori, and K. Hane, J. Opt. Soc. Am. A **18**, 1471 (2001).

[38] I. Celanovic, D. Perreault, and J. Kassakian, Phys. Rev. B **72**, 075127 (2005).

[39] Y. Ueba and J. Takahara, Appl. Phys. Express **5**, 122001 (2012).

[40] Y. Cui, K. H. Fung, J. Xu, H. Ma, Y. Jin, S. He, and N. X. Fang, Nano Lett. **12**, 1443 (2012).

[41] J. A. Bossard, L. Lin, S. Yun, L. Liu, D. H. Werner, and T. S. Mayer, ACS Nano **8**, 1517 (2014).

[42] G. Melentev, V. Shalygin, L. Vorobjev, V. Y. Panevin, D. Firsov, L. Riuttanen, S. Suihkonen, V. Korotyeyev, Y. M. Lyaschuk, V. Kochelap *et al.*, J. Appl. Phys. **119**, 093104 (2016).

[43] D. Costantini, A. Lefebvre, A.-L. Coutrot, I. Moldovan-Doyen, J.-P. Hugonin, S. Boutami, F. Marquier, H. Benisty, and J.-J. Greffet, Phys. Rev. Appl. **4**, 014023 (2015).

[44] H. Chalabi, A. Alù, and M. L. Brongersma, Phys. Rev. B **94**, 094307 (2016).

[45] W. Li and S. Fan, Opt. Express **26**, 15995 (2018).

[46] J.-H. Lee, W. Leung, T. G. Kim, K. Constant, and K.-M. Ho, Opt. Express **16**, 8742 (2008).

[47] C. Wu, N. Arju, G. Kelp, J. A. Fan, J. Dominguez, E. Gonzales, E. Tutuc, I. Brener, and G. Shvets, Nat. Commun. **5**, 3892 (2014).

[48] D. L. C. Chan, M. Soljačić, and J. D. Joannopoulos, Phys. Rev. E **74**, 016609 (2006).

[49] H. Miyazaki, K. Ikeda, T. Kasaya, K. Yamamoto, Y. Inoue, K. Fujimura, T. Kanakugi, M. Okada, K. Hatade, and S. Kitagawa, Appl. Phys. Lett. **92**, 141114 (2008).

[50] W. Li, Z. J. Coppens, L. V. Besteiro, W. Wang, A. O. Govorov, and J. Valentine, Nat. Commun. **6**, 8379 (2015).

[51] N. Shitrit, I. Yulevich, E. Maguid, D. Ozeri, D. Veksler, V. Kleiner, and E. Hasman, Science **340**, 724 (2013).

[52] J. Tian, H. Luo, Q. Li, X. Pei, K. Du, and M. Qiu, Laser Photon. Rev. **12**, 1800076 (2018).

[53] V. A. Fedotov, P. L. Mladyonov, S. L. Prosvirnin, A. V. Rogacheva, Y. Chen, and N. I. Zheludev, Phys. Rev. Lett. **97**, 167401 (2006).

[54] P. N. Argyres, Phys. Rev. **97**, 334 (1955).

[55] J. C. Kemp, J. B. Swedlund, J. Landstreet, and J. Angel, Astrophys. J. **161**, L77 (1970).

[56] J. C. Kemp, Astrophys. J. **162**, 169 (1970).

[57] O. G. Kollyukh, A. I. Liptuga, V. Morozhenko, and V. I. Pipa, Phys. Rev. B **71**, 073306 (2005).

[58] K. Konishi, M. Nomura, N. Kumagai, S. Iwamoto, Y. Arakawa, and M. Kuwata-Gonokami, Phys. Rev. Lett. **106**, 057402 (2011).

[59] S. V. Lobanov, T. Weiss, N. A. Gippius, S. G. Tikhodeev, V. D. Kulakovskii, K. Konishi, and M. Kuwata-Gonokami, Opt. Lett. **40**, 1528 (2015).

[60] S. Lobanov, S. Tikhodeev, N. Gippius, A. Maksimov, E. Filatov, I. Tartakovskii, V. Kulakovskii, T. Weiss, C. Schneider, J. Geßler *et al.*, Phys. Rev. B **92**, 205309 (2015).

[61] A. Demenev, V. Kulakovskii, C. Schneider, S. Brodbeck, M. Kamp, S. Höfling, S. Lobanov, T. Weiss, N. Gippius, and S. Tikhodeev, Appl. Phys. Lett. **109**, 171106 (2016).

[62] A. A. Maksimov, I. I. Tartakovskii, E. V. Filatov, S. V. Lobanov, N. A. Gippius, S. G. Tikhodeev, C. Schneider, M. Kamp, S. Maier, S. Höfling, and V. D. Kulakovskii, Phys. Rev. B **89**, 045316 (2014).

[63] M. Pan, Q. Li, Y. Hong, L. Cai, J. Lu, and M. Qiu, Opt. Express **26**, 17772 (2018).

[64] J. C. W. Lee and C. Chan, Appl. Phys. Lett. **90**, 051912 (2007).

[65] M. Thiel, G. Von Freymann, and M. Wegener, Opt. Lett. **32**, 2547 (2007).

[66] M. Thiel, M. Hermatschweiler, M. Wegener, and G. von Freymann, Appl. Phys. Lett. **91**, 123515 (2007).

[67] J. Hu, X. Zhao, Y. Lin, A. Zhu, X. Zhu, P. Guo, B. Cao, and C. Wang, Sci. Rep. **7**, 41893 (2017).

[68] M. V. Gorkunov, O. Y. Rogov, A. V. Kondratov, V. V. Artemov, R. V. Gainutdinov, and A. A. Ezhov, Sci. Rep. **8**, 11623 (2018).

[69] C. Menzel, C. Rockstuhl, and F. Lederer, Phys. Rev. A **82**, 053811 (2010).

[70] J. A. Bossard and D. H. Werner, Opt. Express **21**, 3872 (2013).

[71] C. Luo, A. Narayanaswamy, G. Chen, and J. D. Joannopoulos, Phys. Rev. Lett. **93**, 213905 (2004).

[72] S. G. Tikhodeev, A. L. Yablonskii, E. A. Muljarov, N. A. Gippius, and T. Ishihara, Phys. Rev. B **66**, 045102 (2002).

[73] M. Moharam, T. Gaylord, E. B. Grann, and D. A. Pommet, J. Opt. Soc. Am. A **12**, 1068 (1995).

[74] D. M. Whittaker and I. S. Culshaw, Phys. Rev. B **60**, 2610 (1999).

[75] R. Messina, A. Noto, B. Guizal, and M. Antezza, Phys. Rev. B **95**, 125404 (2017).

[76] L. Li, J. Opt. Soc. Am. A **13**, 1870 (1996).

[77] S. Tikhodeev, N. Gippius, A. Christ, T. Zentgraf, J. Kuhl, and H. Giessen, Phys. Status Solidi C **2**, 795 (2005).

[78] M. E. Solano, M. Faryad, A. Lakhtakia, and P. B. Monk, J. Opt. Soc. Am. A **31**, 2275 (2014).

[79] L. Li, in *Gratings: Theory and Numeric Applications, Second Revisited Edition*, edited by E. Popov (Institut Fresnel, Marseille, 2014), Chap. 13.

[80] We notice, however, that $\varepsilon_{\text{eff,TM}} = 4.2$ describes the optical resonances of the chiral metasurface better than $\varepsilon_{\text{eff,TM}} = 4.5$ obtained by formula (2). The difference between these values is probably due to the fact that in TM polarization the electric field has a component which is perpendicular to the z axis.

[81] N. A. Gippius, S. G. Tikhodeev, and T. Ishihara, Phys. Rev. B **72**, 045138 (2005).

[82] See Supplemental Material at http://link.aps.org/supplemental/10.1103/PhysRevB.98.235416 for details on the cone representation of electromagnetic field.

[83] U. Fano, J. Opt. Soc. Am. **31**, 213 (1941).

[84] U. Fano, Phys. Rev. **124**, 1866 (1961).